2-Hydroxychromene-2-carboxylic Acid Isomerase: A Kappa Class Glutathione Transferase from *Pseudomonas putida*[†,‡,§]

Lawrence C. Thompson,[||] Jane E. Ladner,[⊥] Simona G. Codreanu,[||] Joel Harp,[||] Gary L. Gilliland,[⊥,#] and Richard N. Armstrong*[,||]

Departments of Biochemistry and Chemistry, Center in Molecular Toxicology, and Center for Structural Biology, Vanderbilt University School of Medicine, Nashville, Tennessee 37232-0146, and Center for Advanced Research in Biotechnology of the Maryland Biotechnology Institute and the National Institutes of Standards and Technology, Gudelsky Drive, Rockville, Maryland 20850

Received February 20, 2007; Revised Manuscript Received April 4, 2007

ABSTRACT: The enzyme 2-hydroxychromene-2-carboxylic acid (HCCA) isomerase catalyzes the glutathione (GSH)-dependent interconversion ($K_{eq} = 1.5$) of HCCA and *trans-o*-hydroxybenzylidene pyruvic acid (tHBPA) in the naphthalene catabolic pathway of *Pseudomonas putida*. The dimeric protein binds one molecule of GSH very tightly ($K_d \approx 5$ nM) and a second molecule of GSH with much lower affinity ($K_d \approx 2$ to 11 μM). The enzyme is unstable in the absence of GSH. The turnover number in the forward direction (47 s^{-1} at 25 °C) greatly exceeds off rates for GSH ($k_{off} \approx 10^{-3}$ to 10^{-2} s^{-1} at 10 °C), suggesting that GSH acts as a tightly bound cofactor in the reaction. The crystal structure of the enzyme at 1.7 Å resolution reveals that the isomerase is closely related to class kappa GSH transferases. Diffraction quality crystals could only be obtained in the presence of GSH and HCCA/tHBPA. Clear electron density is seen for GSH. Electron density for the organic substrates is located near the GSH and is best modeled to include both HCCA and tHBPA at occupancies of 0.5 for each. Although there is no electron density connecting the sulfur of GSH to the organic substrates, the sulfur is located very close (2.78 Å) to C7 of HCCA. Taken together, the results suggest that the isomerization reaction involves a short-lived covalent adduct between the sulfur of GSH and C7 of the substrate.

Glutathione (GSH)[1] transferases are enzymes that catalyze the conjugation of the tripeptide GSH to electrophilic substrates (*1*−*3*). They are present in most aerobic organisms including microorganisms, plants, and animals (*1*, *4*, *5*). The cytosolic or canonical GSH tranferases are the largest group of proteins in the GSH transferase superfamily (*1*−*3*). The proteins are dimers with subunits that contain two domains. The N-terminal domain, which contains the active site, is an archetype fold called the thioredoxin (glutaredoxin) fold (*6*, *7*), whereas the C-terminal domain is all α-helical (*8*). One close relative of the canonical family is the mitochondrial or class kappa GSH transferase family (*3*, *9*−*11*). Proteins of the kappa GSH transferase family also contain a thioredoxin domain and an all α-helical domain; however, their topology is different. The α-helical domain is inserted into the thioredoxin fold (*9*). This discovery shed light on the lack of significant sequence identity between families and suggested that the kappa GSH transferase family evolved on a different path than the canonical family (*9*, *11*).

There are two bacterial proteins to which the kappa GSH transferase shows significant sequence identity; disulfide bond isomerase A (DsbA) and 2-hydroxychromene-2-carboxylic acid (HCCA) isomerase. Although DsbA has the same topology as the kappa GSH transferase (*12*), its active site is fundamentally different. DsbA contains a CXXC motif (Figure 1) in the active site that performs disulfide (redox) chemistry, whereas the kappa GSH transferase has a catalytic serine (S16) at this site that activates GSH for nucleophilic addition reactions (Figure 1) (*9*, *13*). Inasmuch as the

[†] This work was supported by Grants R01 GM30910, P30 ES00267, and T32 ES07028 from the National Institutes of Health.

[‡] The crystallographic coordinates for the structures reported have been deposited with the Protein Data Bank under file names 2IMD and 2IME.

[§] Certain commercial materials, instruments, and equipment are identified in this article to specify the experimental procedure as completely as possible. In no case does such identification imply a recommendation or endorsement by the National Institute of Standards and Technology, nor does it imply that the materials, instruments, or equipment identified are necessarily the best available for the purpose.

* To whom correspondence should be addressed. Tel: (615) 343-2920. Fax: (615) 343-2921. E-mail: r.armstrong@vanderbilt.edu.

[||] Vanderbilt University School of Medicine.

[⊥] Maryland Biotechnology Institute and the National Institutes of Standards and Technology.

[#] Current address: Centocor R&D, Inc., Radnor, PA 19087.

[1] Abbreviations: *P. putida*, *Pseudomonas putida*; *E. coli*, *Escherichia coli*; GSH, reduced glutathione; DsbA, disulfide bond isomerase A; HCCA, 2-hydroxychromene-2-carboxylic acid; tHBPA, *trans-o*-hydroxybenzylidene pyruvic acid; cHBPA, *cis-o*-hydroxybenzylidene pyruvic acid; GS^-, thiolate anion; GSO_3^-, glutathione sulfonate; CDNB, 1-chloro-2,4-dinitrobenzene; DTNB, dithiobis-2-nitrobenzoic acid; PBO, *trans*-4-phenyl-3-buten-2-one; PCR, polymerase chain reaction; OD, optical density; TFA, trifluoroacetic acid; DMSO, dimethyl sulfoxide; LB, Luria broth; CAPS, 2-[*N*-cyclohexylamino]propanesulfonic acid; IPTG, isopropyl-*β*-D-thiogalactopyranoside; HEPES, 4-(2-hydroxyethyl)-1-piperazineethansulfonic acid; EDTA, ethylenediaminetetraacetic acid; DTT, dithiothreitol; Tris, Tris(hydroxymethyl)-aminomethane; SDS−PAGE, sodium dodecyl sulfate−polyacrylamide gel electrophoresis; MALDI, matrix assisted laser desorption ionization; RP-HPLC, reverse phase high pressure liquid chromatography.

10.1021/bi700356u CCC: $37.00
Published on Web 05/18/2007

```
Iso      1 -----MIVDFYFDFLSPFSYLANQRLSKLAQDY-GLTIRYNAIDLARVKIAIGNVGPSNR  54
Kappa    1 MGPAPRVLELFYDVLSPYSWLGFEVLCRYQHLW-NIKLKLRPALLAGIMKDSGNQPP--A  57
DsbA    16 VAGAPQVLEFFS-FFCPHCYQFEEVL----HISDNVKKKL----------------P--E  52

Iso     55 DLKVKLDYLKVDLQRWAQLYGIPLVFPANYNSRRMNIGF-----YYSGAEAQAAAYVNVV 109
Kappa   58 MVPHKGQYILKEIPLLKQLFQVPMSVPKDFFGEHVKKGTVNAMRFLTAVSMEQPEMLEKV 117
DsbA    53 GVKMTKYHV-------------------NFMGGDLGKDLTQAWAVAMALGVE-----DKV  88

Iso    110 FNAVWGEGIAPD---LESLPALVSEKLGWDRSAFEHFL---SSNAATERYDEQTHAAIE 162
Kappa  118 SRELWMRIWSRDEDITESQNILSAAEKAGMATAQAQHLLNKISTELVKSKLRETTGAACK 177
DsbA    89 TVPLFEGV-QKTQTIRSASDIRDVFINAGIKGEEYDAAWNSF---VVKSLVAQQEKAAAD 144

Iso    163 RKVFGVPTMFLGDE----MWW--GNDRLFMLE----ESAMGRLC-RQNADLSS        203
Kappa  178 YGAFGLPTTVAHVDGKTYMLF--GSDRMELLAYLLGEKWMGPVPPTLNARL          226
DsbA   144 VQLRGVPAMF--VNGK-YQLNPQGMDTSNMDVFV--QQYADTVK-YLSEKK          189
```

FIGURE 1: Sequence alignment of the rat kappa GSH transferase with HCCA isomerase (*P. putida*) and DsbA (*E. coli*) using Biology Workbench 3.2 on the San Diego Supercomputer Center website. Identities between kappa and either enzyme are shown in bold. Residues involved in the binding of GSH to the kappa GSH transferase and the corresponding residues in HCCA isomerase are shown in red. The CXXC redox site in DsbA is underlined. The first 15 amino acids of DsbA are not shown because they correspond to a non-aligned N-terminal α-helix (*14*).

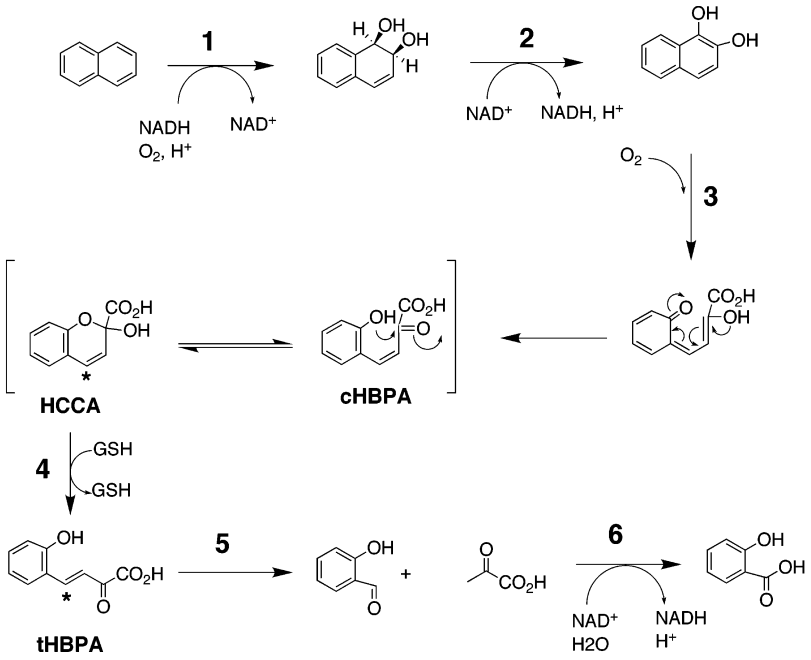

FIGURE 2: Upper naphthalene catabolic pathway from *Pseudomonas putida* (*15*). Step 4 is catalyzed by HCCA isomerase. The asterisk denotes C7 of the substrate.

disulfide chemistry is more like that catalyzed by thioredoxin, DsbA is believed to have arisen prior to the appearance of the kappa GSH transferase (*9*). Even though the sequence identity between the kappa GSH transferase and DsbA or HCCA isomerase is similar (~20% each), alignment of these enzymes (Figure 1) shows that the kappa GSH transferase is more closely related to HCCA isomerase than to DsbA. HCCA isomerase retains all of the residues important for GSH binding (with two minor alterations) including conservation of the catalytic serine residue. In addition, recent modeling results suggest that HCCA isomerase has a kappa-like fold (*14*).

HCCA isomerase is the fourth enzyme in the naphthalene catabolic pathway of *Pseudomonas putida*. During naphthalene utilization, a stable cis isomer, HCCA, is formed from the sterically hindered conformer *cis-o*-hydroxybenzylidene pyruvic acid (cHBPA) when a ketal bond is formed between the phenolic oxygen atom and carbonyl carbon (Figure 2) (*15*). This intermediate is slow to isomerize to its trans counterpart, tHBPA, taking about 6 h to reach equilibrium (*15*). HCCA isomerase increases the rate of approach to equilibrium by several orders of magnitude (*15*, *16*). Interestingly, GSH has been linked to enzyme function (*15*, *16*); however, its exact role in catalysis has remained elusive. Although GSH has been shown to activate the enzyme (*15*, *16*), it has not been clearly demonstrated that GSH is directly involved in chemistry. The product of the reaction is not a GSH conjugate, but it is possible that a covalent intermediate facilitates the isomerization.

Here, we show that HCCA isomerase is a kappa class GSH transferase and suggest a possible GSH dependent enzymatic mechanism. Although the efficiency is low, the enzyme can catalyze the addition of GSH to 1-chloro-2,4-dinitrobenzene (CDNB). In addition, the normal chemistry (Figure 2, step 4) is GSH dependent, suggesting that the enzyme is a GSH transferase. The crystal structure of the protein at

1.7 Å-resolution shows that HCCA isomerase retains the essential features of the kappa fold (2.2 Å rmsd of α-carbons) including the interruption of the thioredoxin fold with the α-helical domain. We postulate that the mechanism of the isomerase involves the covalent addition of GSH to C-7, which changes the hybridization state and facilitates rotation about the double bond.

EXPERIMENTAL PROCEDURES

Materials. GSH, GSO_3^-, TFA, formic acid, $DMSO_{d6}$, salicylaldehyde, pyruvic acid, streptomycin sulfate, EDTA, lysozyme and protease inhibitor cocktail P2714 were purchased from Sigma-Aldrich (St. Louis, MO). Acetonitrile (HPLC grade), H_2O (HPLC grade), and naphthalene were purchased from Fisher Scientific (Pittsburgh, PA). Ampicillin, LB, IPTG, and DTT were purchased from Research Products International (Mt. Pleasant, IL). The pET20b(+) expression vector, the *E. coli* strains BL21(DE3) Tuner and DH5α, the restriction enzymes *EcoR I* and *Xba I*, T4 ligase, and the DNA Wizard kit were purchased from Novagen (Madison, WI). The *E. coli* strain XL-1 Blue was purchased from Stratagene (Cedar Creek, TX). Cloning primers were purchased from Invitrogen (Carlsbad, CA). DEAE Sepharose Fast Flow and Sephacryl 200 were purchased from Amersham Biosciences (Uppsala, Sweden). Crytallography screen Wizard I #27 was purchased from Emerald Biostructures (Bainbridge Island, WA). Plasmids pRE657 and pRE718 (*15*) were gifts from the Environmental Protection Agency. All other chemical reagents were purchased from commercial sources and were used without further purification. All the solutions were prepared and used on the same day. GSH concentrations were measured by titration with DTNB (*17*).

Subcloning, Expression, and Purification of HCCA Isomerase. The HCCA isomerase gene was subcloned from plasmid pRE618 via PCR using the following primers: 5′AAAAAATCTAGACATATGATTGTC-GATTTTTATTTCGAT3′ and 5′AAAAAAGGATCCGAAT-TCTCAACTACTTAAATCGGCATTTTG3′. The PCR product was purified with an agarose gel. Both the PCR product and the plasmid pET20b(+) were digested sequentially with *XbaI* for 2 h and then *EcoRI* overnight. They were ligated with T4 ligase at 15 °C for 16 h. The ligated product was transformed into XL-1 Blue cells, plated onto LB plates containing 100 μg/mL ampicillin, and then placed in an incubator at 37 °C overnight. Using a Wizard kit, DNA was harvested from an overnight culture of one colony from the LB/ampicillin plate. The sequence was confirmed by submission to the Vanderbilt Sequencing Core.

The harvested DNA was transformed into *E. coli* BL-21 (DE3) Tuner cells for protein expression. A glycerol stock of transformed cells was used to inoculate a starter LB culture containing 100 μg/mL ampicillin. The cells were grown for 20 h at 28 °C ($OD_{600} \approx 0.4$) and then used to inoculate 5 × 1 L of LB expression cultures (containing 100 μg/mL ampicillin). The cells were grown in Fernback flasks at 30 °C for 8 h (OD ≈ 0.8) and then cooled to 15 °C. Each culture was induced with 50 μL of l M IPTG for 18 h. Cells were harvested at 7,000*g* for 1 h. The media were removed, and the cells were stored at −80 °C.

Harvested cell pellets were resuspended into 225 mL of 20 mM Tris, 1 mM EDTA, and DTT (pH 7.4) at 25 °C. Then 40 mg of lysozyme was added to the cells, and they were stirred at room temperature for 2 h. Cells were cooled in an ice bath and then lysed with a Bronson sonicator (8 power/70%duty) in 5 × 3 min cycles with 5 min for cooling. Sigma P2714 protease inhibitors were added to the lysate, and then the cell debris was removed at 15,000*g* for 30 min. Supernatant was removed and then treated with 2 g of streptomycin sulfate (in 10 mL H_2O). Precipitate was removed at 15,000*g* for 1 h.

HCCA isomerase was purified on the basis of a previously published protocol (*16*) with the following alterations. The protein was dialyzed, purified, and concentrated at 4 °C unless otherwise noted. The supernatant was dialyzed at 4 °C against 6 L of 100 mM NaCl, 20 mM Tris, 1 mM EDTA, and DTT (pH 7.4) for 24 h and then against 6 L of 20 mM Tris, 1 mM EDTA, and DTT (pH 7.4) for 24 h. The protein was then loaded onto a 450 mL DEAE Sepharose Fast Flow column pre-equilibrated with the same buffer and then washed with 4 L of the same buffer at 1.5 mL/min until the enzyme eluted as the second major peak. All the fractions in that peak were pooled and concentrated to 50 mL in an Amicon concentrator. The protein was dialyzed against 2 L of 50 mM HEPES, 150 mM NaCl, 1 mM EDTA, and DTT (pH 7.0) (storage buffer). The protein was concentrated to 30 mg/mL, and then the protein was loaded in 3 × 2 mL injections onto a 125 mL Sephacryl 200 column pre-equilibrated with the same buffer. The column was washed with buffer at 1 mL/min and 25 °C. Peaks containing the enzyme were pooled and concentrated to 20 mg/mL for storage. The protein was quantified using a calculated extinction coefficient of 41,950 M^{-1} cm^{-1} (*18*). The protein was determined to be pure by visual inspection of a commassie stained SDS−PAGE, and the identity of the protein was confirmed by MALDI mass spectroscopy. Protein was flash frozen on dry ice and then stored at −80 °C. The final yield of protein was approximately 25 mg/L of culture.

Removal of Bound GSH. The enzyme bound GSH was removed from the protein by further dialysis steps following gel filtration. The protein was sequentially dialyzed against 1 M KCl, 50 mM HEPES, 1 mM EDTA, and DTT. Analytical experiments indicated that dialysis for 16 days against 16 × 4 L portions of buffer changed every 24 h was needed to remove most of the GSH from the protein. In a separate preparative experiment, a total of 174 L of buffer and a period of 28 days was needed to remove 93% of the GSH from the protein that was used in the subsequent binding assays. The removal of GSH was confirmed by titration of free thiols (Ellman assay (*17*) in 8 M urea) and by the CDNB/HPLC assay described below.

Analysis of the S-(2,4-Dinitrophenyl)-glutathione Adduct. *S*-(2,4-Dinitrophenyl)-glutathione adducts were loaded (25 μL injections) onto a Beckman-Coulter (Fullerton, CA) 4.6 mm × 250 mm C-18 column and then washed for 5 min with 50 mM sodium acetate at pH 5.0. Peaks were then eluted with a linear gradient of 0%−90% acetonitrile over 10 min and monitored at 340 nm. The *S*-(2,4-dinitrophenyl)-glutathione standard was formed in a reaction of 1 mM GSH and 5 mM CDNB in 200 mM Tris at pH 8.0 at 25 °C for 3 h. The concentration of the adduct was determined at 340 nm (ϵ = 9,600 M^{-1} cm^{-1}) (*19*), and then a standard curve of adduct concentration versus area-under-the-curve was

generated via 25 μL injections of serial dilutions of the *S*-(2,4-dinitrophenyl)-glutathione stock. The amount of GSH remaining in any protein preparation was measured by adding 1 μL of 100 mM CDNB (in ethanol) to 100 μL of protein (200−600 μM range) and allowing it to react for 1 h at room temperature. The reaction was quenched via the addition of 100 μL of chloroform. The sample was vortexed and centrifuged, and then a 25 μL aliquot was analyzed by HPLC.

Synthesis and Purification of HCCA and tHBPA. HCCA and tHBPA were synthesized as stated previously (*15*) with the following alterations. The plasmid pRE657 was transformed into *E. coli* strain DH5α and selected with 100 μg/mL chloramphenicol. Cultures (5 × 1 L) were grown in LB in Fernback flasks at 37 °C to $OD_{600} = 0.8$ and then induced with 1 mM IPTG. Cells were harvested after 2 h of expression at 7000*g* for 30 min (just prior to turning blue). The supernatant was removed, and the cells were stored at −80 °C. The next day, the cells were resuspended into a Fernback flask containing 1 L of M9 salts, 2 mM $MgSO_4$, 0.1 M $CaCl_2$, 25 mM glycerol, and 2 mM $FeSO_4$. The cells were placed at 37 °C for 2 h. Then, 10 mL of 50 mg/mL naphthalene (in ethanol) was added, and the cells were left at 37 °C for 24 h. Formation of HCCA and tHBPA was checked as described previously (*15*). The cells were removed at 7000*g* for 2 h. The supernatant was stored at 4 °C.

The supernatant was extracted with ether, and the organic layer was discarded. The aqueous layer was acidified with 6 M HCl and then extracted again with ether. The ether was removed via rotary evaporation, and the remaining residue was dissolved in a small amount of acetonitrile. The isomers were separated on a Ranin Instrument Company, Inc. (Woburn, MA) Microsorb reverse phase C18/C5 (C18 guard) column with an isocratic gradient of 75% H_2O, 25% actetonitrile, and 0.05% TFA. The elution of the isomers was followed at 256 nm, and the peaks were trapped on dry ice (HCCA elutes first). Each peak was extracted with ether. For elemental analysis, tHBPA (HCCA is not stable as the free acid) was harvested by rotary evaporation of the organic layer followed by drying under vacuum. For kinetic experiments, both molecules were extracted from the organic layer with 100 mM KH_2PO_4 (pH 7.0). The aqueous layer was separated, frozen on dry ice, and then lyophilized to a powder.

Characterization of HCCA and tHBPA. UV−visible spectra were collected on a Perkin-Elmer (Boston, MA) *lambda* 45 double-beam spectrometer. NMR spectra were collected on a Bruker (Germany) 300 MHz NMR spectrometer. Elemental analysis was preformed by Atlantic Microlab, Inc. (Norcross, GA). UV−visible spectra of HCCA and tHBPA were identical to those given in ref *15*. Ratios of ϵ_{256}, ϵ_{296}, and ϵ_{340} were consistent with pure isomers. ^{1}H NMR (300 MHz, 100 mM KH_2PO_4 (pH 7.0 in 50% D_2O) HCCA: δ 5.88, d ($J = 9.8$); δ 6.78, d ($J = 9.8$); δ 6.97, m; δ 7.23, m. tHBPA: δ 6.70, m; δ 6.79, d ($J = 16.4$); δ 7.20, t; δ 7.50, d; δ 7.96, d ($J = 16.4$). Elemental analysis of tHBPA: calcd C = 62.5, H = 4.2, O = 33.3 and found C = 61.8, H = 4.4, O = 32.0.

HCCA Isomerase Activity Assay. The standard assay was carried out at 25 °C and included 20 nM HCCA isomerase, 100 μM GSH, and 920 μM HCCA ($\epsilon_{256} = 7{,}790\ M^{-1}\ cm^{-1}$) (*15*) in 100 mM KH_2PO_4 (pH 7.0). Activity without the addition of GSH was measured at protein concentrations from 200 nM to 2 μM. Product formation was followed at 340 nm ($\epsilon_{340} = 8{,}530\ M^{-1}\ cm^{-1}$) (*15*) in a Perkin-Elmer (Boston, MA) *lambda* 45 double-beam spectrometer. Velocities were calculated from a linear fit of the first 60 s of the reaction and then corrected for background isomerization.

Steady-State Kinetics. All steady-state kinetic measurements were carried out in 100 mM KH_2PO_4 (pH 7.0) at 25 °C. Enzymatic conjugation of GSH and CDNB was measured spectrophotometrically at 340 nm as described previously (*19*). CDNB-dependent kinetic parameters were determined with 1 μM enzyme, 250 μM GSH with [CDNB] varied from 50 μM to 1.0 mM (subsaturating but within the solubility limit). A linear fit of velocity vs [CDNB] was used to determine k_{cat}/K_m^{CDNB}. Kinetics of the HCCA to tHBPA and tHBPA to HCCA isomerization were measured as described above (activity assay) with the following alterations. HCCA isomerase (100 nM final) and GSH (100 μM final) were rapidly mixed with varying concentrations of HCCA (5 to 750 μM final) or tHBPA (10 to 2000 μM final) in an Applied Photophysics Ltd. Model SX17MV stopped-flow spectrometer with a 0.2 cm path-length cell. The concentration dependence of GSH on isomerization was done similarly using HCCA isomerase (100 nM final) and HCCA (920 μM final) while varying the [GSH] (0.5 to 200 μM final). Changes in A_{340} were fit to a single exponential followed by a linear steady state. The constants k_{cat}, K_m, k_{cat}/K_m, and K_i were derived from direct fit of the initial velocities extracted from the linear phase to the Michealis−Menten equation (HCCA and GSH) or the Michaelis−Menten with incomplete substrate inhibition (for tHBPA) (*20*). The dissociation constant, K_d, was determined for HCCA and GSH via a hyperbolic fit to the concentration dependence of the amplitude of the exponential phase of the reaction. All fits were done using the program Prism (Graphpad Software, Inc.). All reactions were corrected for any background reaction.

Kinetics of GSH Binding. Approach to equilibrium kinetic data for GSH binding were obtained on an Applied Photophysics Ltd. Model SX17MV stopped-flow spectrometer with a 0.2 cm path length cell. All experiments were done in 100 mM KH_2PO_4 at pH 7.0 at 10 °C. The rate of appearance (k_{obs}) of the thiolate anion (GS^-) was measured in absorbance mode at 239 nm by mixing HCCA isomerase (10 μM final) with varying [GSH] from 20 to 2000 μM final concentration. An average of 4−6 shots was fit to a double exponential. The off-rate of thiolate anion (GS^-) was determined by measuring the loss of absorbance at 239 nm using a Perkin-Elmer (Boston, MA) *lambda* 45 double-beam spectrometer equipped with a 0.2 cm path length cell. A solution of HCCA isomerase (10 μM final) and GSH (100 μM final) was mixed with GSO_3^- (5 to 200 mM), and the drop in absorbance at 239 nm was fit to a double exponential. Each [GSO_3^-] was repeated in triplicate and averaged together. The change in intrinsic protein fluorescence (k_{obs}) was monitored (excitation at 275 nm and emission above 320 nm) upon mixing HCCA isomerase (500 nM final) with varying [GSH] from 10 to 250 μM final concentration. An average of 4−6 shots was fit to a triple exponential. The final phase (slow phase) of the exponential decay was monitored independent of the first two phases for [GSH] up to 100 mM final concentration. An average of

Table 1: X-ray Data Collection and Processing Statistics

	SeMet (pdb ID 2IMD)	native (pdb ID 2IME)
space group	$P2_12_12$	$P2_12_12$
cell parameters (a, b, c) (Å)	71.34, 76.05, 38.37	71.13, 75.83, 38.30
wavelength of data collection (Å)	1.541	1.541
no. of measured intensities	214,768	798,759
no. of unique reflections (I+ ≠ I−)	53,221	44,029
no. of unique reflections (I+ = I−)		24,499
resolution of data (Å)	1.60	1.70
highest resolution shell (Å)	1.66−1.60	1.76−1.70
R_{sym} (overall/high-resolution shell)	0.043/0.273	0.053/0.273
completeness (%) (overall/high-resolution shell)	100/100	100/100
redundancy (overall/high-resolution shell)	4.04/3.83	18.14/17.47
mean I/σ (overall/high-resolution shell)	16.3/3.4	24.1/8.2

Table 2: Refinement Statistics for Crystal Structures

	SeMet (pdb ID 2IMD)	native (pdb ID 2IME)
resolution limits (Å)	20.0−1.6	20.0−1.7
number of reflections used	26,752	22,223
R-factor (overall/high-resolution shell)	0.187/0.331	0.186/0.263
R_{free} (overall/high-resolution shell)	0.226/0.404	0.235/0.353
non-protein molecules (not water)	1 glutathione, 1 CAPS, 2 PO_4^{-2}, ligand, product	1 glutathione, 1 CAPS, 2 PO_4^{-2}, ligand, product
no. of water molecules	215	158
rms deviation bond length (Å)	0.020	0.022
rms deviation angle (°)	1.90	1.95
average B main chain/side chain/water (Å^2)	19.9/21.9/33.1	23.0/25.6/34.6

4−6 shots was fit to a single exponential (when the first 2 s of the reaction were discarded).

Crystallization. All crystals were grown under 7 mL of Al's oil in a 72 well microbatch plate from Hampton Research (Laguna Niguel, CA). Protein/ligand stock was mixed 1:1 (3 μL each) with Emerald Biostructures (Bainbrigde Island, WA) Wizard I #27: 1.2 M NaH_2PO_4, 0.8 M K_2HPO_4, 0.2 M $LiSO_4$, and 0.1 M CAPS (pH 6.1). The crystal trays were stored at 21 °C. Crystals normally grew in 1 to 2 weeks. Stocks of native protein (and selenomethione protein) with GSH and HCCA/tHBPA were made as follows: the protein was thawed on ice and then mixed with GSH and HCCA to a final concentration of 10 mg/mL protein, 1 mM GSH, and 1 mM HCCA (in the storage buffer). Crystals were removed from the drop and dipped into a cryoprotectant solution (80% Wizard #27 and 20% ethylene glycol) just prior to mounting on the X-ray goniometer and flash cooling in the cold flow.

X-ray Data Collection and Processing. Data for the native crystals were collected using a Rigaku R-Axis IV image plate area detector on a Rigaku RU-200 rotating anode X-ray generator operated at 5.0 kW. Crystals were maintained at 100 K using an X-Stream cryostat. Data for the selenomethione crystal were collected using a Rigaku Micro Max 007 rotating anode generator and a Rigaku RAXIS IV^{++} detector (Rigaku/MSC, The Woodlands, TX). The crystal was cooled to 106 K with a Rigaku Xtream 2000 cryocooler. The diffraction data for the native and selenomethione crystals were processed with CrystalClear/d*Trek. The data collection and processing statistics are shown in Table 1.

Structure Determination. The structure was solved using the technique of single isomorphous replacement combined with single wavelength anomalous dispersion. The polypeptide has 6 methionines and a total length of 203 residues. The Matthews coefficient assuming one molecule in the asymmetric unit is 2.22. X-ray data sets for a native and a selenomethione crystal were both collected at 1.541 Å. Six Se sites were identified with the program SOLVE (*21*), and the initial figure of merit was 0.45 to 2.0 Å. RESOLVE (*22*) was used in an iterative script (www.solve.lanl.gov) with REFMAC5 (*23*) to build the initial model using the selenomethionine data. The best model was built in cycle 9; it included 175 residues with side chains identified for 170 of the residues. The overall *R* factor for this model was 0.339, and the $R_{free}$was 0.365. The model was completed in cycles of viewing and modeling with XtalView (*24*) and refining with REFMAC5. The final model includes all of the residues (1−203), one molecule of glutathione, one molecule of CAPS, two partial occupancy phosphate ions, partially occupied ligand and product in the active site, and 215 water molecules. Using sigma-a weighted $F_o - F_c$ difference maps as a guide, the occupancy for the selenium atoms was set at 0.8 for all of the selenomethionine residues. The native structure was determined by transferring the partially refined selenomethionine protein structure without any waters or ligands to the native data and using REFMAC5 to refine and XtalView to visually adjust the model and inspect the fit to the electron density map. The final model includes all of the residues, one molecule of glutathione, one molecule of CAPS, two partially occupied and one fully occupied phosphate ion, a partially occupied ligand and product in the active site, and 158 water molecules. In both refinements, the density in the active site was not modeled until near the end of the refinement in order to be able to interpret it without biasing the interpretation. The final refinement statistics for both structures are shown in Table 2.

RESULTS

Steady-State Kinetics of HCCA Isomerase with GSH and CDNB, HCCA, or tHBPA. The enzyme showed a low but significant GSH transferase activity toward CDNB (Table 3). Because of the low affinity of the enzyme for

Table 3: Kinetic and Affinity Parameters of Substrates for HCCA Isomerase[a]

	k_{cat} (s^{-1})	K_m (μM)	k_{cat}/K_m (M^{-1} s^{-1})	K_i (μM)	K_d (μM)
$CDNB_{(GSH)}$			200 ± 7		
$HCCA_{(GSH)}$	47 ± 2	84 ± 10	$5.6 \pm 0.7 \times 10^5$		19 ± 5
$tHBPA_{(GSH)}$	19 ± 7	138 ± 72	$1.3 \pm 0.9 \times 10^5$	136 ± 100	
$GSH_{(HCCA)}$	39 ± 1	17 ± 2	$2.3 \pm 0.3 \times 10^6$		14 ± 3

[a] The subscripts in parentheses indicate the secondary substrate that is held at a constant, saturating concentration.

Table 4: Activity of Recombinant HCCA Isomerase

added cofactor	specific activity (μmol s^{-1} mg^{-1})
none (prior to removal of GSH)	$4.5 \pm 0.5 \times 10^{-2}$
none (after removal of GSH)	$1.0 \pm 0.1 \times 10^{-2}$
1 mM GSO_3^-	$1.5 \pm 0.7 \times 10^{-3}$
100 μM GSH	1.3 ± 0.1

CDNB and the solubility limits of the compound, saturation with CDNB was not possible. Consequently, nonlinear regression analysis of the initial velocity data was not possible; therefore, linear methods were used to determine steady-state parameters. The efficiency of the isomerase in this reaction (Table 3) is 2 orders of magnitude lower than that for the kappa GSH transferase (*9*). An estimate of the upper limit of the turnover number of about 2 s^{-1} was obtained by Lineweaver−Burk analysis through extrapolation to the *y*-intercept ($1/V_{max}$). The low turnover number of the enzyme in the CDNB reaction suggested the possibility that product release might be the rate-limiting step. This possibility was dismissed when transient state kinetic experiments showed no burst phase for the enzymatic progress curve (data not shown).

Previous work indicated that S16 of the kappa GSH transferase participated in catalysis by facilitating the ionization of the sulfhydryl group of GSH (*9*). Sequence alignments suggested that S11 (Figure 1) should have the same role in HCCA isomerase. The S11A mutant was created but no soluble protein could be extracted from the bacteria to test enzymatic activity.

Once the natural substrate was available, measurement of native enzyme kinetics was possible. Because of the background reaction of GSH with product (tHBPA) and the enzymatic conversion of product back to substrate, HCCA, tHBPA, and GSH dependent kinetics were carried out using a stopped-flow spectrophotometer. Upon mixing HCCA or tHBPA with 100 nM enzyme and 100 μM GSH or mixing GSH with 100 nM enzyme and 1 mM HCCA, the absorbance at 340 nm increased for reactions in which [HCCA] or [GSH] was varied and decreased for reactions in which [tHBPA] was varied. These traces were fit to a model of a single exponential followed by a steady state (eq 1). The velocity of the steady state increased with increasing [substrate] and fit well to a Michaelis−Menten model for reactions in which HCCA or GSH was varied or a Michaelis−Menten model with incomplete substrate inhibition (eq 2, where *b* varies from 0 to 1 with 0 = complete inhibition) (*20*) for the reaction in which [tHBPA] was varied. The amplitude of the exponential phase showed a hyperbolic dependence on concentration for reactions in which HCCA and GSH were varied. The concentration dependences fit well to a single site binding hyperbola (eq 3), yielding both K_m and K_d in one experiment (Table 3).

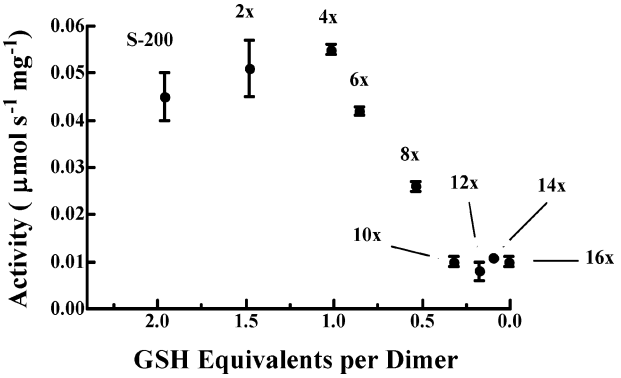

FIGURE 3: Enzyme activity as a function of GSH equivalents measured during dialysis against 1 M KCL. Each dialysis step was against 4 L of 1 M KCl for 24 h. The enzyme was assayed for residual GSH and catalytic activity every 2 days for a total of 16 days. The plot is labeled to indicate the number of dialysis steps of the enzyme after initial gel filtration (S-200).

$$A_{340} = Ae^{-kt} + mx + c \quad (1)$$

$$m = [(V_{max}{*}X)(1 + b{*}X/K_i)]/[K_m + X + (X^2/K_i)] \quad (2)$$

$$A = (B_{max}{*}X)/(K_d + X) \quad (3)$$

Multiple wavelength stopped-flow analysis of the exponential phase for both HCCA dependent reactions yielded an extracted UV spectrum that correlated to the product tHBPA (data not shown); however, the extinction coefficient of the change in amplitude is much too large to be the build up of product in the active site from a single turnover and is more consistent with multiple turnovers of the enzyme during the exponential phase. The build up of product may be the result of a slow onset of inhibition by tHBPA.

GSH and HCCA Isomerase Chemistry. The exact role of GSH in the HCCA isomerase reaction has been an enigma. Glutathione has been variously suggested to activate the enzyme, stabilize it, or otherwise be essential for efficient catalysis (*15*, *16*, *25*). One possible source of this ambiguity is the presence of GSH in the purified enzyme. The recombinant enzyme has significant catalytic activity without the addition of exogenous GSH as indicated in Table 4. In addition, the presence of GSH in the enzyme preparation was detected by titration of the purified protein with DTNB in the Ellman assay (*17*). The identity of the thiol was determined to be GSH by detection of a conjugate of GSH with CDNB formed upon mixing the purified enzyme with CDNB, vortexing with chloroform, and then analyzing the sample by HPLC. A peak eluted corresponding to a *S*-(2,4-dinitrophenyl)-glutathione standard.

The bound GSH can be removed from the purified enzyme by extensive dialysis of the protein preparation against 1 M KCl as illustrated in Figure 3. The concentration of GSH (using the CDNB/HPLC assay) and the corresponding enzymatic activity were monitored during the dialysis. The results indicate that the loss of one equivalent of GSH per dimer was accomplished after only four rounds of dialysis and had little effect on the residual activity (Figure 3). The last equivalent was more difficult to extract taking 12

additional dialysis steps and showed a 5-fold drop in activity (Table 4 and Figure 3). The activity of the apo enzyme was still 7-fold higher than that of the enzyme in the presence of the inhibitor GSO_3^- (Table 4 and Figure 3). GSO_3^- binds to the active site, displacing GSH. Addition of 100 μM GSH at any time before or after the removal of GSH restored native activity that was 29-fold higher than that of the enzyme prior to the removal of GSH by dialysis (Table 4).

Additional apo protein was prepared for GSH binding experiments. Prior to dialysis against 1 M KCl, both the Ellman (*17*) and CDNB/HPLC assays showed 1.8 ± 0.1 equiv of GSH present per dimer. Following dialysis against a total of 174 L of 1 M KCl over a period of 28 days, both assays indicated the presence of 0.14 ± 0.01 equiv of GSH per dimer. Significantly, the removal of GSH was accompanied by the loss of ~50% of the protein by precipitation. To avoid further loss of protein, dialysis was halted. Subsequent binding experiments were conducted with protein that contained 0.07 equiv of GSH per active site.

Kinetics of GSH Binding to HCCA Isomerase. The presence of approximately two equivalents of GSH per dimer in the enzyme preparation even after gel filtration suggested that the enzyme binds the ligand very tightly. The first trials at measuring the binding kinetics of GSH failed because of the instability and precipitation of the apo enzyme at 25 °C. In contrast, when experiments were conducted at 10 °C, precipitation was no longer a problem, and the experiments proceeded normally.

Upon mixing HCCA isomerase with GSH, there is an increase in absorbance at 239 nm, consistent with the formation of thiolate in the active site (Figure 4A) (*26*). The absorbance increase fit well to a two-exponential expression (Figure 4A). A plot of k_{obs} versus [GSH] shows linear correlation for both exponentials, consistent with the two-step binding model (Scheme 1), and yielded bimolecular rate constants (k_1 and k_2) for both steps (Table 5). The intercepts for both fits were slightly negative with large errors indicating that the off-rate constants for both steps (k_{-1} and k_{-2}) are very small compared to the corresponding on-rate constants (Table 5). The amplitude of the signal for step 1 was consistently ~25% less than step 2 with the amplitude corresponding to an extinction coefficient of 3,500 M^{-1} cm^{-1} for the thiolate chromophore. The latter observation is consistent with the partial occupancy of one site in the enzyme preparations used for the experiments.

The off-rate for the thiolate anion was measured by trapping the free enzyme with GSO_3^- after rapid mixing of GSO_3^- with HCCA isomerase pre-loaded with GSH. The absorbance at 239 nm decreased in a biphasic manner that fit well to a double exponential expression (Figure 4B). The k_{obs} and the amplitude for the first exponential showed a linear relationship to [GSO_3^-] with negative and positive slopes, respectively. This is consistent with a two-step model for the loss of the first thiolate (Scheme 2) in which a slow conformational change occurs prior to thiolate leaving the active site. In this case, the slope and intercept (of k_{obs} vs [GSO_3^-]) gave k_3 and k_{-3}, respectively (Table 5). The k_{obs} and the amplitude for the second exponential showed no dependence on [GSO_3^-], consistent with a single step (Scheme 3), and provided a direct measure of the off-rate of the second thiolate when one site is occupied with GSO_3^- (Table 5). The amplitude of the second exponential corresponded to an extinction coefficient of 5,000 M^{-1} cm^{-1} for the second thiolate. With this additional information the GSH binding model in Scheme 1 was revised to the model given in Scheme 4.

Upon mixing HCCA isomerase with GSH, the intrinsic protein fluorescence increased and then decreased (Figure 4C and D). The increase in fluorescence fit well to a double exponential expression, whereas the decrease fit well to a single exponential (Figure 4C and D). This result is consistent with the three-step binding model proposed in Scheme 4. The k_{obs} for the first two exponentials of the changes in fluorescence exhibited a linear dependence on [GSH] and yielded the bimolecular rate constants (k_1 and k_2) for both steps that are in reasonable agreement with those obtained in the absorbance experiments (Table 5). The first exponential again gave a slightly negative intercept with a high error, indicating that k_{-1} is significantly smaller than k_1. However, the second exponential showed a good fit with a positive intercept and yielded a reasonable measure of k_{-2} (Table 5).

The final exponential (slow phase) took >100 s to reach equilibrium and showed no dependence of k_{obs} on [GSH] over the range of concentrations suitable to fit all three phases together. In order to determine whether the slow phase showed a concentration dependence, it was monitored independent of the other phases (the first two became too fast to measure) at [GSH] up to 100 mM (Experimental Procedures). The kinetics exhibited a very slight concentration dependence (~0.03 to ~0.06 s^{-1}), consistent with a unimolecular approach to equilibrium that is much slower than the preceding step. In this instance, the $k_{obs} \approx k_3 + k_{-3}$. The estimate of $k_{-3} + k_3$ is in good agreement with the rate constants obtained from the global modeling of the fluorescence data (Table 5).

The change in intrinsic protein fluorescence was globally modeled to Scheme 4 using the program Dynafit (Figure 4D). The rate constants for all steps as well as the response/quantum yield for the first two steps were allowed to float. Because of the slow nature of the final step in relationship to the time window of the experiments (100 s window and a $k_{obs} \approx 0.03$ s^{-1}), the Dynafit program had trouble fitting the quantum yield of this step; therefore, it was fixed at 0.2. The results gave good correlation to the overall model including good residuals for both *x* and *y* coordinates (data not shown). The quantum yield of step 1 was 0.40 ± 0.1, whereas that for step 2 was 0.70 ± 0.01. This correlates to a 43% smaller quantum yield for step 1 than for 2. This result is similar to that seen for the A_{239} binding experiments (where the extinction of step 1 was ~25% smaller than that of step 2), again suggesting that all residual GSH is bound in only one active site. The resulting rate constants (Table 5) showed an acceptable correlation to those extracted from absorbance and fluorescence measurements. The major exception was k_{-1}. The program tried to drive the value of k_{-1} to zero (Table 4). This is not unexpected considering that the very low off-rate for the step (Table 5) is to small to be accurately measured within the 100 s window for the data collection. The fit estimated the value of k_{-1} to be about 2 orders of magnitude smaller than was suggested by the GSO_3^- trapping experiment. This is not unexpected considering that the fluorescence modeled k_{-1} is the off-rate of GSH with the other active site empty (Scheme 4), whereas the A_{239} trapping

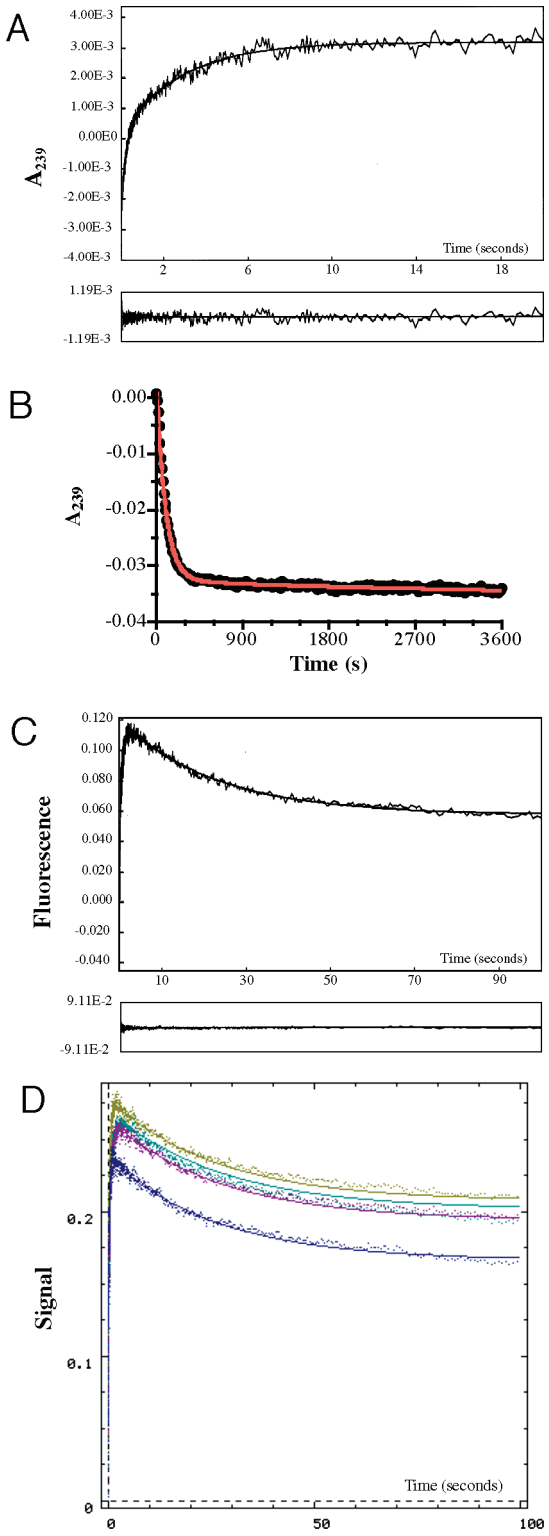

FIGURE 4: Approach to equilibrium measurements for the binding of GSH to HCCA isomerase. (Panel A) Increase in A_{239} upon mixing 40 μM GSH and 10 μM HCCA isomerase. (Panel B) A_{239} decrease upon mixing 10 μM HCCA isomerase loaded with 100 μM GSH with 200 mM GSO_3^-. Data from panels A and B are fit to double exponentials. (Panel C) Changes in intrinsic protein fluorescence upon mixing 40 μM GSH with 0.5 μM HCCA isomerase. Data from panel C are fit to a triple exponential expression. (Panel D) Changes in intrinsic protein fluorescence upon mixing 30 μM (cyan), 50 μM (magenta), 80 μM (yellow) and 150 μM (blue) GSH with 0.5 μM HCCA isomerase. The data from panel D are fit to the model in Scheme 4 using the program Dynafit. The fitting parameters (rate constants) derived for all experiments are provided in Table 5.

Scheme 1

$$E + GSH \underset{k_{-1}}{\overset{k_1}{\rightleftharpoons}} E{\bullet}GS^- + GSH \underset{k_{-2}}{\overset{k_2}{\rightleftharpoons}} E{\bullet}2GS^- + 2H^+$$

experiment is the off-rate with GSO_3^- in the opposite site (Scheme 3). Global fitting of the data with k_{-1} fixed at zero gave rate constants (data not shown) similar to those given in Table 5.

Using the on- and off-rate constants extracted from the various experiments, apparent dissociation constants were calculated for each bound GSH molecule (Table 6). Values for the low affinity site are in fair agreement with each other and with the dissociation constant measured for GSH in the burst/steady-state experiments (Table 3). The least confident value is that generated for the K_d of the high affinity site due to the uncertainty in the measurement of k_{-1}. It should be emphasized that k_{-1} from the A_{239} experiments is the off-rate with GSO_3^- bound and not an empty opposing active site, and the resulting K_d should be considered an upper limit of the high affinity site binding constant. A better measurement, even though it has a very high error, is the high affinity site dissociation constant calculated from the fluorescence modeling (Table 6). It is 2 orders of magnitude tighter, and almost all of this difference results from the much smaller k_{-1} (Table 5).

Overall Structure of HCCA Isomerase. The crystal structure of HCCA isomerase in the presence of substrate was solved at a resolution of 1.7 Å. The final refinement statistics for the model are given in Table 2. The asymmetric unit contained a single monomer of the enzyme, one molecule of GSH, and a mixture of HCCA and tHBPA. Gel filtration studies (data not shown) indicate that the native enzyme is a dimer; therefore, the dimer was reconstructed using the appropriate symmetry operations. The topology of the HCCA isomerase (Figure 5A) is similar to that of the kappa GSH transferase (Figure 5B) as was previously predicted on the basis of a homology model (*14*). The thioredoxin fold is interrupted by the insertion of an α-helical domain. The rmsd between the α-carbons of the monomers of the enzymes is 2.2 Å (Figure 5C). The computer models predicted that HCCA isomerase would have a helix preceding the thioredoxin fold (*14*). This is not the case.

The structure reveals two major differences between the kappa GSH transferase and the isomerase. The first difference is an additional helix in the helical domain of kappa (F87-K94) appears as a loop in the HCCA isomerase (A82-N85) (Figure 5C). The second difference is located at the C-terminus. The final helix of the thioredoxin domain of HCCA isomerase continues almost to the C-terminus of the protein, whereas this helix is much shorter in the kappa protein with a longer loop structure extending to the C-terminus (Figure 5C).

Structure of the GSH Binding Site. The crystal structure confirms that the GSH binding residues conserved in the sequence alignment (Figure 1) are involved in the binding of GSH to HCCA isomerase. These include S11, V168 (main-chain N and CO), N48, N181, and D182 from the host monomer as well as K59 and R183 that reach across the dimer interface (Figure 6). There are differences in the GSH binding site that yield two additional interactions between the isomerase and GSH not found in the kappa GSH

Table 5: Rate Constants for the Binding and Dissociation of GSH with HCCA Isomerase

rate constant (units)	linear regression of k_{obs} vs [GSH] for A_{239}	loss of A_{239} via GSO_3^- trapping	linear regression of k_{obs} vs [GSH] for fluorescence	slow phase from fluorescence data	global modeling of fluorescence data
k_1 ($M^{-1}s^{-1}$)	$(2.0 \pm 0.1) \times 10^5$		$(5.5 \pm 0.6) \times 10^5$		$(3.8 \pm 0.2) \times 10^5$
k_{-1}(s^{-1})	-7 ± 6[a]	$(9.0 \pm 6.0) \times 10^{-4}$	-0.4 ± 0.6[a]		$(1.9 \pm 2.7) \times 10^{-5}$
k_2 ($M^{-1}s^{-1}$)	$(1.5 \pm 0.1) \times 10^4$		$(2.7 \pm 0.1) \times 10^4$		$(3.2 \pm 0.2) \times 10^4$
k_{-2}(s^{-1})	-7 ± 8[a]		0.3 ± 0.1		0.05 ± 0.04
k_3(s^{-1})		0.054 ± 0.015			0.022 ± 0.001
k_{-3}(s^{-1})		0.020 ± 0.002			0.016 ± 0.002
$k_3 + k_{-3}$ (s^{-1})		0.074 ± 0.015		$\sim$0.03−0.06	0.038 ± 0.002

[a] The negative intercepts are due to the fact that the rate constants for the off-reactions are close to zero. These numbers are included solely to indicate that the actual rate constants cannot be determined within the precision of the data for these experiments.

Scheme 2

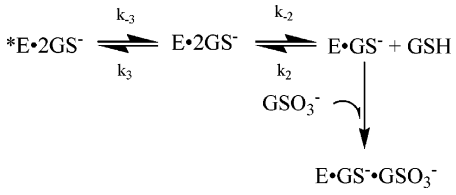

Scheme 3

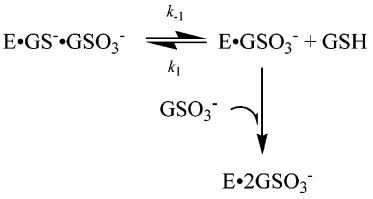

Scheme 4

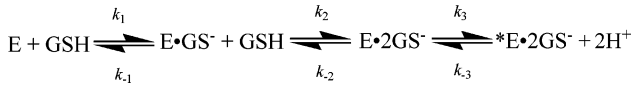

Table 6: Calculated Dissociation Constants for High and Low Affinity GSH Binding Sites

method	high affinity (μM)	low affinity (μM)
A_{239} on and off rates	0.005 ± 0.003	
fluorescence on and off rates		11 ± 4
modeling of fluorescence data		2 ± 1

transferase. The first of these arises from the indole N-H of W179 (F in the kappa GSH transferase) donating an additional hydrogen bond to the cysteinyl carbonyl group (Figure 6). The second comes from the presence of an additional water molecule. In the kappa GSH transferase, the side chain of S200 interacts directly with the carboxyl end of the γ-glutamate (*9*). There is a conservative change in HCCA isomerase to asparagine at this position (Figure 1). N181 uses its main chain N-H to interact with the carboxyl end of γ-glutamate, while its side chain (along with main chain N of D182 and the side chain of R183) orients a H_2O molecule that also hydrogen bonds to the carboxyl end of the γ-glutamate. The overall gain from W179 and the ordered H_2O represent two additional hydrogen-bonding partners to GSH.

Active Site and the Presence of Substrate. The presence both GSH and HCCA/tHBPA were absolutely required for crystallization of the protein. Examination of the region near the active site reveals extra electron density that is consistent with the presence of substrate/product in the active site of the enzyme and is shown in Figure 7A. This electron density could not be fit well to either HCCA or tHBPA alone; however, a model that included both HCCA and tHBPA at an occupancy of 0.5 for each gave a reasonable fit to the electron density. In addition, the cysteinyl side chain of GSH appears in two conformations that may reflect two organic species in the active site very close to the SH group of GSH.

The far end of the active site contains a group of hydrophobic side chains that forms a pocket that accepts the aromatic end of HCCA (Figure 7B). The opposing side of the active site is capped by a series of polar/charged side chains that hydrogen bond to the charged ends of both HCCA and tHBPA (Figure 7B and C). In addition, the carboxyl group of tHBPA has an interaction with the main-chain N-H of the glycyl residue of GSH (Figure 7C). The side chain sulfhydryl of GSH is modeled in two conformations. One conformation is within hydrogen-bonding distance of the hydroxyl group of S11 (2.61 Å in Figure 7B), whereas the other is further away (3.28 Å in Figure 7C). The conformation of the cysteinyl side chain is most likely influenced by the ligand that is present in the active site (Figure 7B, HCCA or Figure 7C, tHBPA). In the conformation more distant from S11, the sulfur atom is $\sim$2 Å from C7 of HCCA. Considering that there is little or no electron density between these atoms, the result suggests either a bad contact or a conformation that is only present in active sites containing tHBPA (Figure 7C). This does not rule out the possibility that the sulfur atom assumes this conformation during a transient covalent bond between GSH and C7 of HCCA that is not so highly populated in the complex.

DISCUSSION

GSH and HCCA Isomerase Chemistry. The ability of HCCA isomerase to catalyze the conjugation of GSH and CDNB, albeit at a low rate, indicates that the enzyme activates GSH toward nucleophilic addition reactions and suggests that the normal chemistry of the isomerase reaction might involve a GSH conjugate. The normal chemistry of the enzyme does show dependence on [GSH] that follows Michaelis−Menten kinetics (Table 3). This includes an overall activation of 145-fold over the apo enzyme (Table 4). The GSH-dependent activation has been observed previously (*15*, *16*, *25*), but its catalytic role remained elusive. The addition of the inhibitor, GSO_3^-, results in an almost

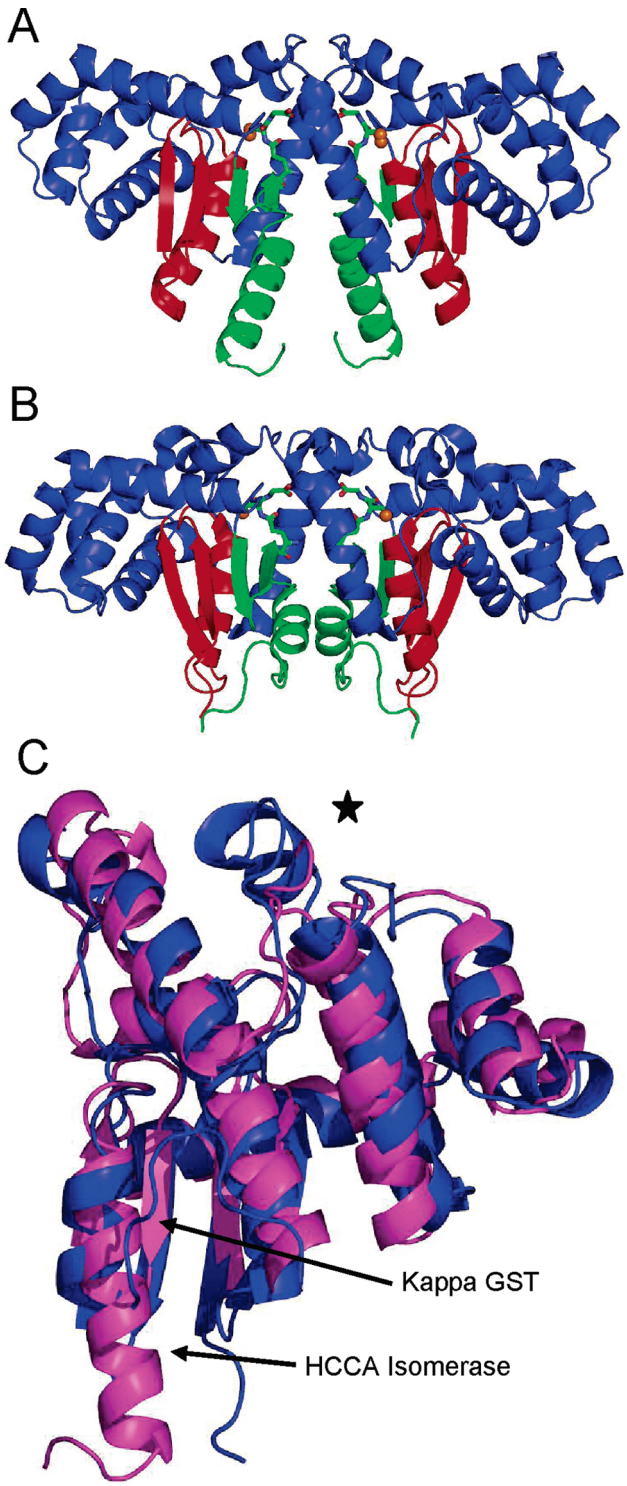

FIGURE 5: Ribbon diagram of the HCCA isomerase dimer (A) and kappa GST dimer (B) including GSH as a stick model with the cysteinyl sulfur colored orange (sulfur has two conformations in HCCA isomerase). The N-terminal $\beta\alpha\beta$ (red) and C-terminal $\beta\beta\alpha$ (green) motifs that make up the thioredoxin domain as well as the intervening all helical domain (blue) show the conservation of the kappa GSH transferase fold/topology in the HCCA isomerase structure. (C) Overlay of the individual monomers from HCCA isomerase (magenta) and kappa GSH transferase (blue). The two major structural differences between the enzymes are an extra helix (indicated by the star) in the helical domain of kappa GSH transferase and a loop (the kappa GSH transferase) versus helix (HCCA isomerase) at the C-terminus (indicated by arrows). All images were created in PYMOL (*27*), and the overlay was done with DALI (*28*).

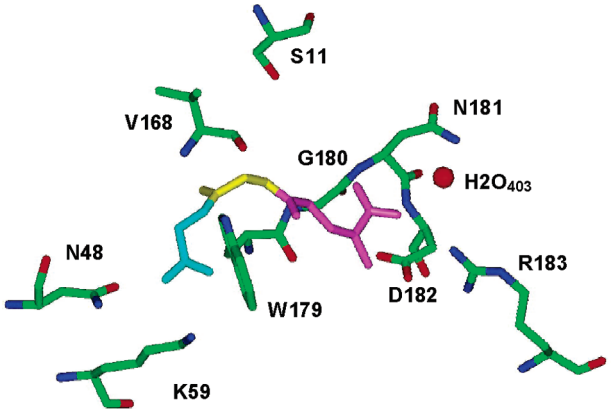

FIGURE 6: GSH binding residues in HCCA isomerase. The three residues of GSH are color coded as glycine (cyan), cysteine (yellow), and γ-glutamate (magenta). G180 does not interact with GSH. The cysteine side chain of GSH (two conformations) has been removed for clarity. This Figure was created with the program Insight (*29*).

complete loss of catalytic activity (Table 4), indicating a direct involvement of the cysteinyl sulfur in catalysis at the active site. Inasmuch as the apo protein shows a 7-fold higher activity than that of the enzyme with inhibitor bound (Table 4), it appears that the active site maintains some catalytic potential beyond that donated by GSH.

Complexity of the Binding of GSH. The detection of GSH after the final purification step (Figure 3) suggests that the protein has a very high affinity for the ligand. The inability to easily remove all of the GSH even with extensive dialysis against high salt concentrations is a clear indication that the affinity is much higher than that which is typical (10 to 100 μM) for canonical or class kappa GSH transferases (*1*, *3*, *9*, *30*). Approach to equilibrium binding measurements are consistent with this conclusion, suggesting that the highest affinity site has a dissociation constant in the mid pM to low nM (Table 6). It is noteworthy, however, that the lower affinity site falls within the typical affinity range (Table 6) and that maximum activity is not achieved until this site is saturated (Tables 3 and 4).

HCCA isomerase exhibits negative cooperativity in the binding of GSH (Figure 4, Scheme 4, and Tables 4 and 5), a characteristic that is atypical for canonical or kappa GSH transferases (*1*, *3*, *9*, *30*). The only GSH transferase known to show cooperative GSH binding is the microsomal enzyme, MGST1 (*31*−*33*). This protein is a membrane-bound trimer that binds GS^- at one site and GSH at the remaining two weak sites (*34*). The cooperativity observed in HCCA isomerase is not entirely unexpected considering the close approach of GSH molecules in the structure (Figure 5A). In retrospect, it is surprising that the kappa GSH transferase does not exhibit cooperativity because the locations of the GSH molecules are almost identical (Figure 5B).

Kappa Fold and the Binding of GSH. Canonical GSH transferases typically have about a dozen interactions with GSH (*30*), generating dissociation constants within the range given above. The mammalian kappa class enzyme has only eight polar interactions between the peptide and the protein (*9*) and has a K_d at the high end of that range. In contrast, HCCA isomerase has two additional interactions (Figure 6) that appear to contribute to the high affinity site in the isomerase that are not observed in the kappa GSH transferase

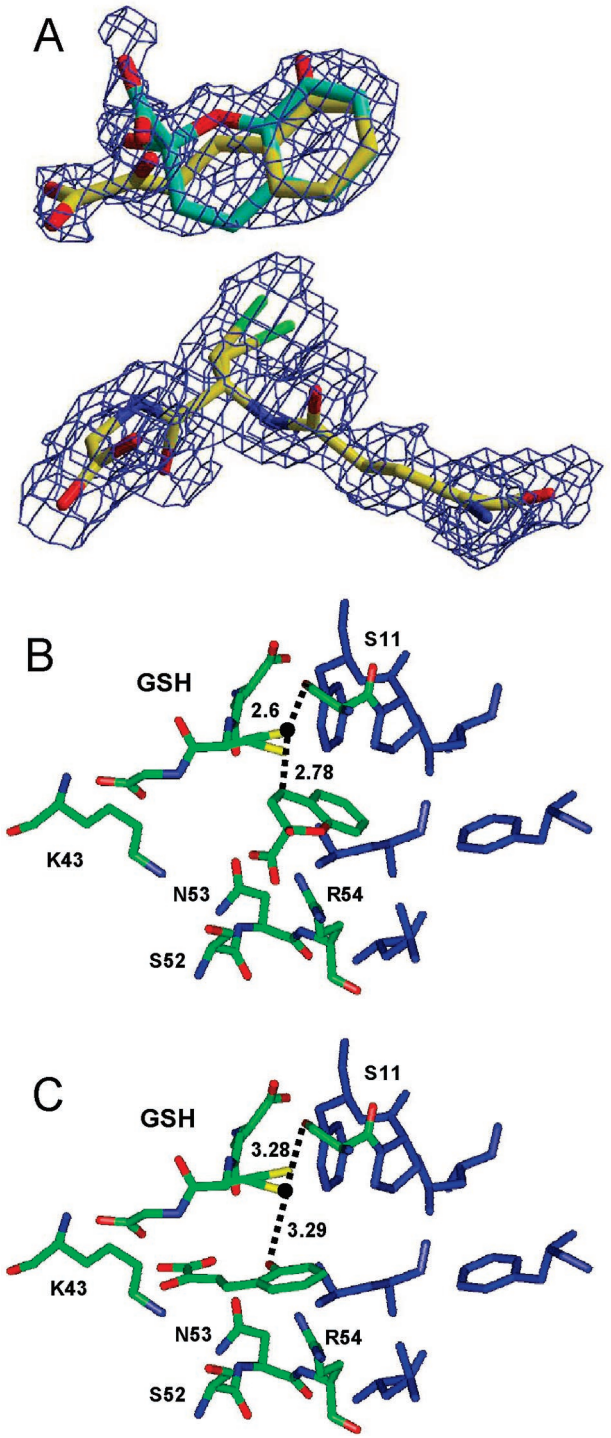

FIGURE 7: Residues in the active site of HCCA isomerase, P12, F13, L60, L63, L67, and F80 (blue), form a hydrophobic binding pocket to accept the aromatic end of HCCA while K43, S52, N53, and R54 interact with the charged groups on HCCA and/or tHBPA (colored by atom and labeled by residue). (Panel A) Sigma a-weighted $2mF_o - DF_c$ map with a contour level of 0.6σ and the electron density of the active site containing GSH, HCCA (cyan), and tHBPA (yellow). (Panels B and C) HCCA and tHBPA, respectively, alone in the active. These panels include the distance from the cysteinyl sulfur to S11 and C7 (B) or the aromatic hydroxyl group (C). Panels B and C where created with the program Insight (*29*).

(Table 5). Clearly, the isomerase exploits structural characteristics that result in additional binding energy upon association with GSH.

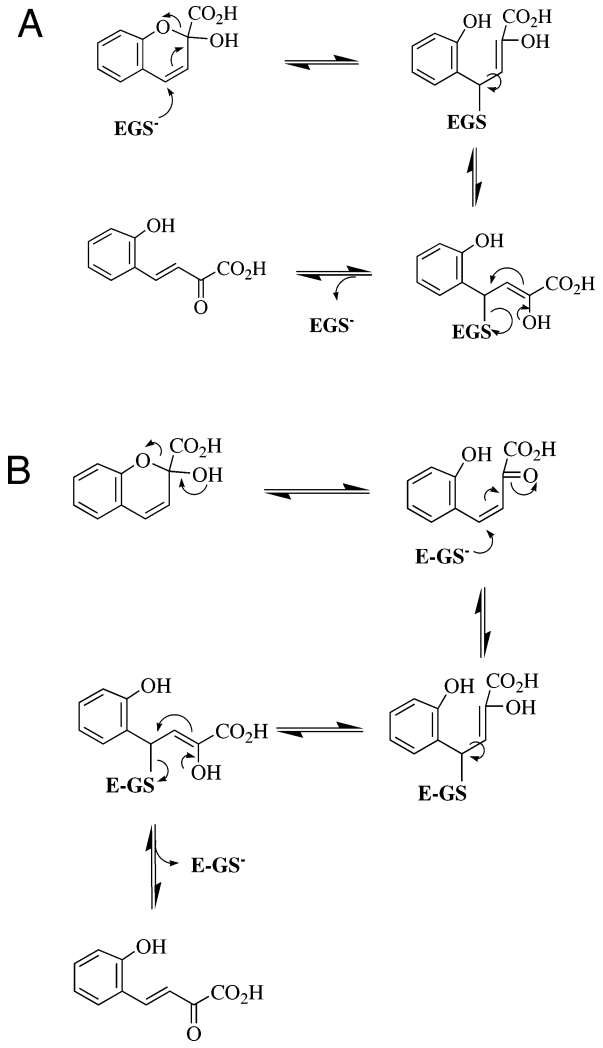

FIGURE 8: Proposed enzymatic mechanisms of HCCA isomerase. Both mechanisms involve the nucleophillic attack of GSH at C7 that leads to the formation of a covalent intermediate that facilitates free rotation around the C7−C8 bond. Elimination of GSH in a retro-Michael reaction yields the tHBPA product. (Panel A) Conjugate addition mechanism in which GSH addition and ring opening occur concomitantly. (Panel B) Ordered mechanism in which the ring opens and then GSH adds in a 1,4-Michael fashion.

GSH and the Stability of HCCA Isomerase. The apo enzyme with no GSH bound exhibits a diminished stability. This is consistent with previous observations (*15*) that suggested that GSH also performs a structural role in the enzyme. The varying extent of catalytic enhancement by exogenous GSH reported in the literature and in this work could be partially a result of a more ordered active site as well as the addition of a nucleophile for catalysis. Interestingly, there are no reports that indicate a loss of structural integrity for an apo kappa GSH transferase.

GSH as a Cofactor in the Isomerase Reaction. Inasmuch as the enzymatic product is not a GSH conjugate, it is difficult to unequivocally demonstrate that GSH is directly involved in catalysis. Moreover, the tight binding of GSH suggests that even if a transient adduct is formed in the reaction, it may not be released from the active site. The activation of the enzyme by GSH and the near complete inhibition by GSO_3^- strongly suggest that the thiol or thiolate of GSH is involved in chemistry. However, the low activity of the enzyme with one molecule of GSH bound per dimer

and the instability of the enzyme in the absence of GSH suggests that stabilization of the active site is also a major contributor to the activation. If GSH directly participates in catalysis, the most likely scenario would involve a nucleophilic attack at C7 in a Michael or pseudo-Michael conjugate addition (Figure 8). The addition would alter the hybridization at C7 and decrease the C7−C8 bond order to promote rotation about the bond. The crystal structure shows that the sulfur of GSH is in good position to attack C7 of HCCA even though the electron density of the region suggests that the active site is occupied by more than one species (Figure 7).

The lack of significant electron density between the sulfur of GSH and C7 suggests that the conjugate addition product (if formed) is a species that is not highly populated in the active site of the crystal. However, the electron density of the organic substrate indicating an equal population of both isomers of the substrate in the active site suggests an internal equilibrium constant of one, consistent with efficient catalysis. The observations in the crystal are also consistent with the transient spectral behavior in solution. The addition of GSH to either HCCA or tHBPA results in a rapid increase in absorbance during the initial phase of the reaction. The addition of GSH to C7 of either substrate would be expected to cause an initial decrease in absorbance in the UV spectrum of both HCCA and tHBPA. The lack of a transient decrease in absorbance is consistent with either no intermediate or one that is too short-lived to be detected in the stopped-flow.

If a Michael or conjugate addition product is formed, it could either decompose on the protein surface or depart the active site before decomposing in solution. The latter scenario seems unlikely because of the transient nature of the Michael or conjugate addition product that might be formed and the slow off-rates observed for GSH. For example, the off-rate constant even for the low affinity GSH site (0.3 s^{-1} at 10 °C, Table 4) is much lower than the turnover number of the enzyme (47 s^{-1} at 25 °C, Table 3).

Proposed Mechanisms for HCCA Isomerase. In order for the isomerization reaction to proceed, two key events must occur. First, the hybridization at C7 of HCCA must change from sp^2 to sp^3 to allow free rotation around the C7−C8 bond. Second, the ketal bond between O1 and C9 must be broken. The order in which these events occur, however, is unknown. There are two possible GSH dependent mechanisms that satisfy both of these criteria and are consistent with the data presented here. The first is a concerted conjugate addition mechanism in which GSH adds to C7 altering the hybridization at the carbon with concomitant breaking of the ketal bond (Figure 8A). The alternative is an ordered mechanism in which a transiently formed ring-opened intermediate (cHBPA) is attacked by the sulfur nucleophile (Figure 8B). Both of these mechanisms facilitate a change to sp^3 hybridization at C7 and promote free rotation about the C7−C8 bond. The $E{\cdot}GS^-$ complex is then eliminated in a retro-Michael reaction, freeing the product (tHBPA) to exit the active site (Figure 8).

The second mechanism may be more likely due to the characteristics of the intermediate formed after ring opening and the principle of microscopic reversibility. This molecule (cHBPA) is a precursor in the formation of HCCA (Figure 2) during the catabolism of naphthalene and has been detected in equilibrium mixtures of HCCA and tHBPA (*15*). Its structure is very similar to that of *trans*-4-phenyl-3-buten-2-one (PBO), a known GSH transferase substrate (*35*−*37*). GSH transferase reactions with PBO are 1,4-Michael additions of GSH to the electrophile. This is the same GSH addition reaction suggested in Figure 8B. Moreover, the mechanism is very similar to that proposed for maleylacetoacetate isomerase (*38*, *39*).

Relationship of HCCA Isomerase and the Kappa Glutathione Transferase. The structural relationship between HCCA isomerase and kappa GSH transferase firmly places the enzyme into the kappa family of enzymes; however, it does not reveal a concise evolutionary relationship. Both proteins could have evolved separately from DsbA (their most likely progenitor). Finally, HCCA isomerase represents yet another example of a bacterial enzyme involved in the catabolism of xenobiotics that is related to mammalian proteins involved in the metabolism of toxic molecules.

ACKNOWLEDGMENT

The *Pseudomonas putida* DNA was a gift from Dr. Richard Eaton (Environmental Protection Agency).

REFERENCES

1. Armstrong, R. N. (1997) Structure, catalytic mechanism, and evolution of the glutathione transferases, *Chem. Res. Toxicol. 10*, 2−18.
2. Hayes, J. D., Flanagan, J. U., and Jowsey, I. R. (2005) Glutathione transferases, *Annu. Rev. Pharmacol. Toxicol. 45*, 51−88.
3. Pearson, W. R. (2005) Phylogenies of glutathione transferase families, *Methods Enzymol. 401*, 186−204.
4. Vuilleumier, S., and Pagni, M. (2002) The elusive roles of bacterial glutathione S-transferases: new lessons from genomes, *Appl. Microbiol. Biotechnol. 58*, 138−146.
5. Edwards, R., Dixon, D. P., and Walbot, V. (2000) Plant glutathione S-transferases: enzymes with multiple functions in sickness and in health, *Trends Plant. Sci. 5*, 193−198.
6. Katti, S. K., LeMaster, D. M., and Eklund, H. (1990) Crystal structure of thioredoxin from *Escherichia coli* at 1.68 Å resolution, *J. Mol. Biol. 212*, 167−184.
7. Bushweller, J. H., Billeter, M., Holmgren, A., and Wuthrich, K. (1994) The nuclear magnetic resonance solution structure of the mixed disulfide between *Escherichia coli* glutaredoxin (C14S) and glutathione, *J. Mol. Biol. 235*, 1585−1597.
8. Xia, B., Vlamis-Gardikas, A., Holmgren, A., Wright, P. E., and Dyson, H. J. (2001) Solution structure of *Escherichia coli* glutaredoxin-2 shows similarity to mammalian glutathione-S-transferases, *J. Mol. Biol. 310*, 907−918.
9. Ladner, J. E., Parsons, J. F., Rife, C. L., Gilliland, G. L., and Armstrong, R. N. (2004) Parallel evolutionary pathways for glutathione transferases: structure and mechanism of the mitochondrial class kappa enzyme rGSTK1-1, *Biochemistry 43*, 352−361.
10. Harris, J. M., Meyer, D. J., Coles, B., and Ketterer, B. (1991) A novel glutathione transferase (13-13) isolated from the matrix of rat liver mitochondria having structural similarity to class theta enzymes, *Biochem. J. 278*, 137−141.
11. Pemble, S. E., Wardle, A. F., and Taylor, J. B. (1996) Glutathione S-transferase class Kappa: characterization by the cloning of rat mitochondrial GST and identification of a human homologue, *Biochem. J. 319*, 749−754.
12. Martin, J. L., Bardwell, J. C. A., and Kurylan, J. (1993) Crystal structure of the DsbA protein required for disulphide formation *in vivo*, *Letters to Nature 365*, 464−468.
13. Fabianek, R. A., Hennecke, H., and Thony-Meyer, L. (2000) Periplasmic protein thiol:disulfide oxidoreductases of *Escherichia coli*, *FEMS Microbiol. Rev. 24*, 303−316.
14. Robinson, A., Huttley, G. A., Booth, H. S., and Board, P. G. (2004) Modelling and bioinformatics studies of the human Kappa-class glutathione transferase predict a novel third glutathione transferase

family with similarity to prokaryotic 2-hydroxychromene-2-carboxylate isomerases, *Biochem. J. 379*, 541−552.
15. Eaton, R. W., and Chapman, P. J. (1992) Bacterial metabolism of naphthalene: construction and use of recombinant bacteria to study ring cleavage of 1,2-dihydroxynaphthalene and subsequent reactions, *J. Bacteriol. 174*, 7542−7554.
16. Ohmoto, T., Kinoshita, T., Moriyoshi, K., Sakai, K., Hamada, N., and Ohe, T. (1998) Purification and some properties of 2-hydroxychromene-2-carboxylate isomerase from naphthalenesulfonate-assimilating *Pseudomonas* sp. TA-2, *J. Biochem. (Tokyo) 124*, 591−597.
17. Ellman, G. L. (1959) Tissue sulfhydryl groups, *Arch. Biochem. Biophys. 82*, 70−77.
18. Edelhoch, H. (1967) Spectroscopic determination of tryptophan and tyrosine in proteins, *Biochemistry 6*, 1948−1954.
19. Habig, W. H., and Jakoby, W. B. (1981) Assays for differentiation of glutathione-S-transferases, *Method Enzymol. 77*, 398−405.
20. Wang, J., Araki, T., Ogawa, T., Matsuoka, M., and Fukuda, H. (1999) A method of graphically analyzing substrate-inhibition kinetics, *Biotechnol. Bioeng. 62*, 402−411.
21. Terwilliger, T. C., and Berendzen, J. (1997) Bayesian MAD phasing, *Acta Crystallogr., Sect. D 53*, 571−579.
22. Terwilliger, T. C. (2003) Automated main-chain model building by template matching and iterative fragment extension, *Acta Crystallogr., Sect. D 59*, 38−44.
23. Murshudov, D. N., Vagin, A. A., and Dodson, E. J. (1997) Refinement of macromolecular structures by the maximum-likelihood method, *Acta Crystallogr., Sect. D 53*, 240−255.
24. McRee, D. E. (1999) *Practical Protein Crystallography*, 2nd ed., Academic Press, San Diego, CA.
25. Kuhm, A. E., Knackmuss, H. J., and Stolz, A. (1993) 2-Hydroxychromene-2-carboxylate isomerase from bacteria that degrade naphthalenesulfonates, *Biodegradation 4*, 155−162.
26. Graminski, G. F., Kubo, Y., and Armstrong, R. N. (1989) Spectroscopic and kinetic evidence for the thiolate anion of glutathione at the active site of glutathione S-transferase, *Biochemistry 28*, 3562−3568.
27. Delano, W. L. *PYMOL*, The PyMOL Molecular Graphics System, De Lano Scientific, Palo Alto, CA, http://www.pymol.org.
28. Holm, L., and Sander, C. (1993) Protein structure comparison by alignment of distance matrices, *J. Mol. Biol. 233*, 123−138.
29. *Insight II*, Accelrys Inc., San Diego, CA, http://www.accelrys.com/products/insight/.
30. Dirr, H., Reinemer, P., and Huber, R. (1994) X-ray crystal structures of cytosolic glutathione S-transferases. Implications for protein architecture, substrate recognition and catalytic function, *Eur. J. Biochem. 220*, 645−661.
31. Jakobsson, P. J., Morgenstern, R., Mancini, J., Ford-Hutchinson, A., and Persson, B. (2000) Membrane-associated proteins in eicosanoid and glutathione metabolism (MAPEG). A widespread protein superfamily, *Am. J. Respir. Crit. Care Med. 161*, S20−S24.
32. Jakobsson, P. J., Morgenstern, R., Mancini, J., Ford-Hutchinson, A., and Persson, B. (1999) Common structural features of MAPEG − a widespread superfamily of membrane associated proteins with highly divergent functions in eicosanoid and glutathione metabolism, *Protein Sci. 8*, 689−692.
33. Bresell, A., Weinander, R., Lundqvist, G., Raza, H., Shimoji, M., Sun, T. H., Balk, L., Wiklund, R., Eriksson, J., Jansson, C., Persson, B., Jakobsson, P. J., and Morgenstern, R. (2005) Bioinformatic and enzymatic characterization of the MAPEG superfamily, *FEBS J. 272*, 1688−1703.
34. Morgenstern, R., Svensson, R., Bernat, B. A., and Armstrong, R. N. (2001) Kinetic analysis of the slow ionization of glutathione by microsomal glutathione transferase MGST1, *Biochemistry 40*, 3378−3384.
35. Chen, J., and Armstrong, R. N. (1995) Stereoselective catalysis of a retro-Michael reaction by class mu glutathione transferases. Consequences for the internal distribution of products in the active site, *Chem. Res. Toxicol. 8*, 580−585.
36. Kubo, Y., and Armstrong, R. N. (1989) Observation of a substituent effect on the stereoselectivity of glutathione S-transferase toward para-substituted 4-phenyl-3-buten-2-ones, *Chem. Res. Toxicol. 2*, 144−145.
37. Habig, W. H., Pabst, M. J., and Jakoby, W. B. (1974) Glutathione S-transferases. The first enzymatic step in mercapturic acid formation, *J. Biol. Chem. 249*, 7130−7139.
38. Seltzer, S. A. M. L. (1979) Maleylacetone *cis-trans*-isomerase. Mechanism of the interaction of coenzyme glutathione and substrate maleylacetone in the presence and absence of enzyme, *J. Am. Chem. Soc. 101*, 3091−3097.
39. Polekhina, G., Board, P. G., Blackburn, A. C., and Parker, M. W. (2001) Crystal structure of maleylacetoacetate isomerase/glutathione transferase zeta reveals the molecular basis for its remarkable catalytic promiscuity, *Biochemistry 40*, 1567−1576.

BI700356U